Int. J. Metrol. Qual. Eng. **16**, 9 (2025)

https://doi.org/10.1051/ijmqe/2025009

International Journal of Metrology and Quality Engineering

Available online at:
www.metrology-journal.org

RESEARCH ARTICLE OPEN ACCESS

Nonlinear active disturbance rejection control for industrial robotic arm and its application

Zhiwei Geng[1] and Teng Wan[2,*]

[1] Engineering Training and Innovation Center, Zhengzhou University of Industrial Technology, Zhengzhou, 451100, PR China
[2] College of Mechanical and Control Engineering, Baicheng Normal University, Baicheng, 137000, PR China

Received: 14 May 2025 / Accepted: 13 August 2025

Abstract. Industrial robotic arms are widely used, but they face control challenges in complex environments due to strong joint coupling, nonlinear dynamics, uncertain parameters, and external disturbances. Traditional control methods struggle to provide high precision and robustness under these conditions. Therefore, a nonlinear Active Disturbance Rejection Control (ADRC) method is proposed. This approach takes an extended state observer to estimate and compensate for total disturbances, enhancing accuracy and robustness. Experimental results show that the proposed method significantly improves response performance. In response to a step signal, the system shows clear dynamic changes. Under sine excitation, z1 and z2 closely match the input, while z3 shows minimal response. Compared to the traditional sliding mode control, which shows obvious error peaks and fluctuations (0.035–0.05 rad) at 10–15 s, the nonlinear ADRC sliding mode control achieves 30% faster response speed, 60% smaller overshoot, and more stable performance with errors consistently below 0.01 rad. This method effectively observes state variables and disturbances, optimizing motion control and offering a reliable solution for high-performance control of industrial robotic arms.

Keywords: Industrial robotic arm / nonlinear ADRC / ESO / nonlinear state error feedback / tracking differentiator

1 Introduction

Industrial robot arms are a key component in the field of industrial robotics, defined as automated devices that simulate human arm movements. These robotic arms are renowned for their high versatility, flexible mobility, excellent obstacle avoidance performance, and convenient maneuverability. They have been widely used in various industrial applications, including material handling, welding operations, painting processes, and cutting operations [1]. Due to the expanded production scale and diversified application environments, the operating environment of industrial robot arms has expanded from open spaces to confined spaces filled with obstacles. This technology has been proven to liberate human operators from dangerous and monotonous tasks, thereby improving the efficiency of the production process [2]. In this environment, academic attention has shifted towards path planning. The development of obstacle avoidance planning technology is of particular significance. The performance of this technology is directly related to the manipulation effect of the robot arm. Meanwhile, traditional static planning algorithms are difficult to address existing problems, and there is currently relatively little research on dynamic obstacle avoidance planning for robotic arms [3]. There are various interference factors in dynamic environments, such as the vibration of the robotic arm, external impacts, and uncertainty of obstacle positions. These interference may cause the robotic arm to deviate from the path planned for obstacle avoidance. Active Disturbance Rejection Control (ADRC) can compensate for these interference, enhancing the anti-interference ability of the robotic arm. The robotic arm must be able to track the path set by the obstacle avoidance plan with the highest accuracy. ADRC has been extensively applied in permanent magnet linear synchronous motor drive systems due to the strong anti-interference ability and fast response speed. However, some parameter adjustments have added difficulties to its application.

To address the issues discussed, Yuan C et al. proposed a sliding mode-based self-correcting parameter self-impedance control. Sliding Mode (SM) was combined Extended State Observer (ESO) to achieve parameter self-tuning. The proposed control method reduced jitter effects, exhibited excellent anti-interference performance, and provided fast dynamic response [4]. The European Control Association robot manipulator has been widely used in

* Corresponding author: Teng.wwan@outlook.com

modern industry. The end effector needs to move precisely along a given trajectory. Ben M. S. et al. built a robust feedback control method to deal with this issue. The controller exhibited superiority in satisfying stability and target value requirements [5]. Nuo E et al. proposed a distributed control method with a proportional-integral-derivative scheme structure that is easy to implement. The controller used an internal model approach to suppress disturbances [6]. Switching systems often involve models that are difficult to determine. Flores Padilla M. et al. developed an adaptive controller for nonlinear discrete-time switching systems. The experimental results showed that the proposed controller exhibited closed-loop performance on discrete-time switching and disturbed systems [7].

Based on geometric feedforward controller, Xie H et al. proposed a path tracking framework based on composite interference suppression, which combined cascaded active interference suppression controller and online estimator. Especially, model-based cascaded ADRC consisted of an outer loop controller and an inner loop controller. In addition, to improve transient response, a geometric feedforward controller based on parameter self-learning was built. The effectiveness was evaluated, proving its superiority over traditional pure tracking algorithms [8]. The impact of pressure shock disturbance generated by the supply pump on the tracking performance of hydraulic robotic arms has been proven to be an important issue. To address this challenge, Yao S et al. proposed an impact disturbance compensation controller, which was developed to handle uncertainty and pressure impact disturbances in hydraulic systems. The experimental results indicated that the controller provided a theoretical guarantee for the asymptotic tracking performance of hydraulic manipulators under uncertainty and mixed disturbances. In addition, the maximum tracking error and average variance of Proportional-Integral-Derivative (PID) were reduced by 68.7% [9]. The mathematical model and optimal modulation scheme of Dual-Active Hybrid Full-Bridge (H-FDAB) Direct Current − Direct Current (DC-DC) Converter have not been fully explored. Luo S et al. proposed a DC-DC converter return power optimization strategy based on ADRC. The experiment ultimately proved the effectiveness and practicality of the designed control strategy. This method effectively solved the challenges of inherent converter efficiency reduction and output voltage fluctuations in the converter. Under traditional Proportional-Integral (PI) control, this converter generated a large amount of return power [10]. To avoid unnecessary movement and save energy, Jing A et al. built a correction adaptive ADRC. This new algorithm could be used for pitch angle control of underwater gliders. The ADRC could compensate for control inputs [11].

In summary, researchers have conducted some research on the control technology of industrial robotic arms, including ADRC, sliding mode self-tuning parameters, robust feedback control methods, composite interference suppression, and high-precision tracking control. However, the application of dynamic obstacle avoidance planning, parameter adaptive control, anti-interference ability, system stability, and optimization is not deep enough. Therefore, a control method for industrial robotic arms based on nonlinear ADRC technology is proposed, which innovatively adopts an improved ESO and integrates new functions to achieve efficient nonlinear control, providing a technical basis for control improvement of industrial robotic arms.

The article structure is as follows. The first part focuses on the industrial robotic arm control method based on nonlinear ADRC technology. The second part specifically verifies the proposed algorithm. The third part draws conclusions and shortcomings of this design and the directions that need to be further explored in the future.

2 Methods and materials

A control method for industrial robotic arms based on nonlinear ADRC technology is built. Firstly, the nonlinear ADRC technology is adopted and the ESO is improved. Secondly, the study applies the proposed improved nonlinear ADRC technology to industrial robotic arms and analyzes the control effectiveness.

2.1 Nonlinear ADRC technology based on improved SMESO

With the increasingly complex application environment and expanding industrial production of robotic arms, traditional control methods have been unable to meet the growing demand for industrial applications. Exploring the control method has become a popular development trend. ADRC technology was proposed in 1998. Its core idea is to consider the internal and external uncertainty factors as total disturbances, and estimate and compensate for them through ESO [12,13]. This method does not rely on the precise mathematical model, making ADRC perform well in controlling complex systems with nonlinearity, time-varying, and unknown disturbances. ADRC technology estimates the internal uncertainty and external disturbances by introducing ESO, and then takes a state feedback controller for accurate adjustment [14]. This technology not only significantly improves control accuracy, but also enhances the efficiency of the entire production process by reducing response time. Figure 1 displays the ADRC structure.

In Figure 1, $r(t)$ is the system reference input signal, and $\dot{r}(t)$ is the differential signal of the reference input; $y(t)$ is the output of the controlled object, and $y_0(t)$ is the output feedback signal processed by the First order filter; $w(t)$ is an external disturbance; Z_1, Z_2, Z_3 are the state observation values output by Nonlinear Extended State Observer, corresponding to different states of the system; Nonlinear combination is used to perform nonlinear processing on the error signal to obtain the intermediate control variable u_0; $1/b$ and b are control gain related parameters, and after calculation, the final control quantity u is output to act on the Controlled object, achieving control and disturbance suppression of the system. ADRC has three parts. The tracking differentiator can smooth the input signal, extract the differential signal, and arrange the transition process to avoid overshoot, solving the noise sensitivity in traditional

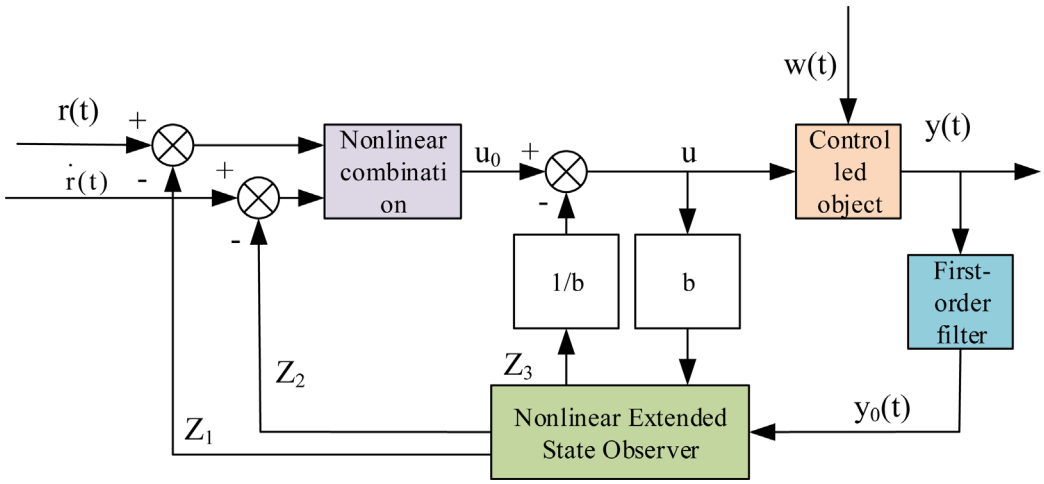

Fig. 1. Structure diagram of ADRC.

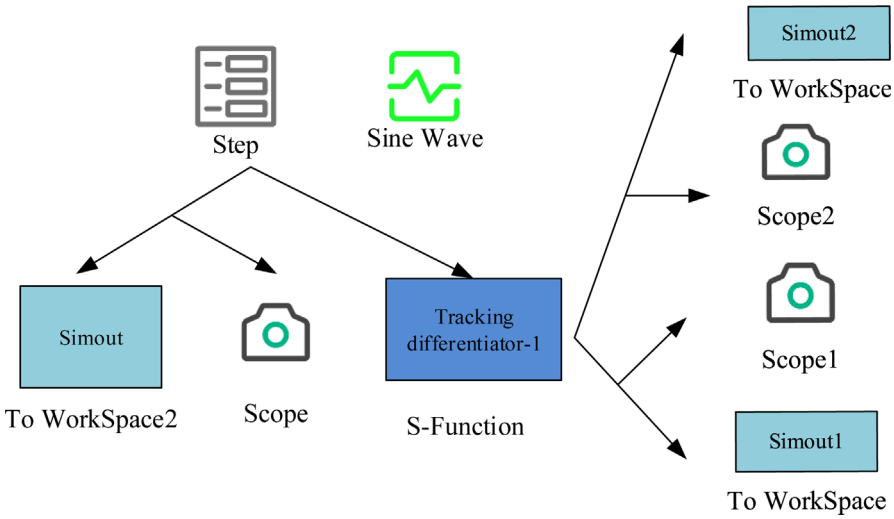

Fig. 2. Simulink simulation diagram of tracking differentiator.

differentiators and providing smooth input signals and their derivatives [15]. ESO can estimate state variables and total disturbances (including internal and external disturbances) of the system, treating the unknown dynamics and external disturbances as "extended states" and conducting online estimation through observers [16]. The Nonlinear State Error Feedback (NLSEF) Control Law can generate control signals through nonlinear combinations based on state errors and disturbance estimates, utilizing nonlinear characteristics to improve the dynamic response and disturbance rejection capability. Figure 2 displays the Simulink simulation diagram of the tracking differentiator.

In Figure 2, the tracking differentiator is a signal preprocessing algorithm used to extract smooth signals and their derivatives from noisy signals. The tracking differentiator algorithm is shown in equation (1).

$$\begin{cases} fh = fhan(v_1(k) - v(k), v_2(k), r_0, h_0) \\ v_1(k+1) = v_1(k) + hv_2(k) \\ v_2(k+1) = v_2(k) + hfh \end{cases} \quad (1)$$

In equation (1), h represents the sampling period. r_0 signifies the speed factor. $fhan(v_1,\ v_2,\ r_0,\ h_0)$ represents the fastest control function. h_0 represents the filtering factor. $v_1(k)$ represents the tracking signal at time k, $v_2(k)$ represents the derivative of the tracking signal at time k, and fh represents the output of the fastest control function. Nonlinear function is an important core component of ADRC, as shown in equation (2).

$$\mathrm{fal}(e, \alpha, \delta) = \begin{cases} |e|^{\alpha}\mathrm{sign}(e) & |e| > \delta \\ \dfrac{e}{\delta^{1-\alpha}} & |e| \le \delta \end{cases}. \quad (2)$$

In equation (2), δ represents the filtering factor. α represents the non-linear factor. e represents the tracking error. Mechanical systems generally exhibit strong nonlinearity, and traditional linear control methods are difficult to accurately describe these characteristics, resulting in model mismatch and decreased control accuracy. Therefore, a novel nonlinear function is selected for the study, as

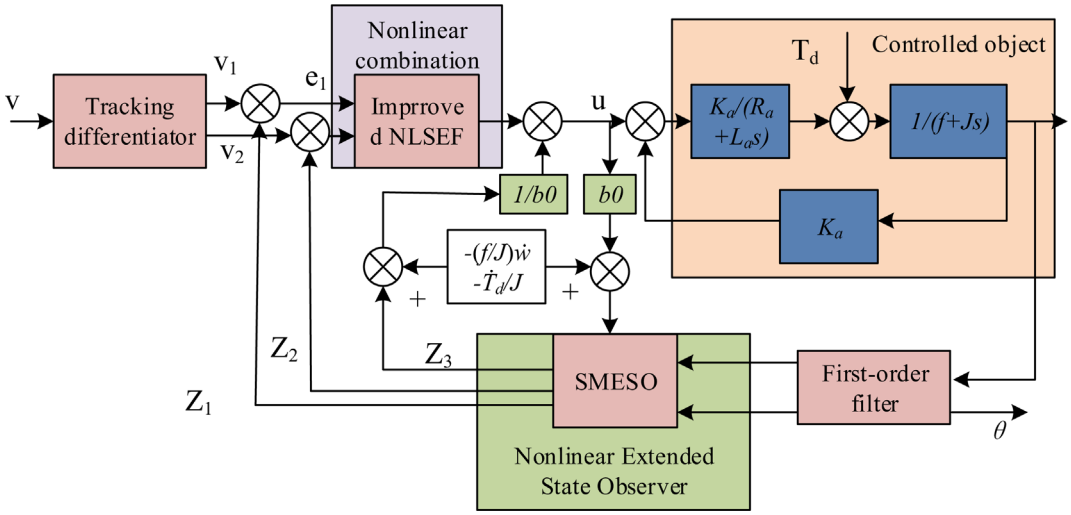

Fig. 3. Structure diagram of improved nonlinear ADRC.

shown in equation (3).

$$nf(e,\alpha,\delta)=\begin{cases}|e|^{\alpha}sign(e) & |e|>\delta\\ m_1e+m_2e^2+m_3\tan e & |e|\le\delta\end{cases}. \tag{3}$$

In equation (3), m_1, m_2, and m_3 represent joint mass parameters. The traditional ESO calculation is presented in equation (4).

$$\begin{cases}e_1=z_1-y\\ \dot{z}_1=z_2-\beta_1e_1\\ \dot{z}_2=z_3-\beta_2nf(e_1,\alpha_0,\delta_1)+b_0u\\ \dot{z}_3=-\beta_3nf(e_1,\alpha_1,\delta_1)\end{cases}. \tag{4}$$

In equation (4), z_1 represents the tracking signal of output y. β_1, β_2, and β_3 represent the gain coefficients. e_1 represents the tracking error. z_2 represents the differential signal of y. b_0 represents the estimated compensation coefficient. z_3 represents the observed total disturbance. α_0 and α_1 represent nonlinear factors. δ_1 represents the filtering factor.

The study adopts a Sliding Mode ESO (SMESO), which can better achieve good evaluation performance with lower efficiency and handle uncertainty and external disturbances. Firstly, the sliding surface is shown in equation (5).

$$\begin{cases}s=\dot{\tilde{e}}+\Lambda\tilde{e}\\ e=q-z_1\end{cases}. \tag{5}$$

In equation (5), s represents the sliding surface. $\Lambda\in R^{3\times3}$ represents a diagonal positive definite matrix, and $s=[\,s_1\quad s_2\quad s_3\,]^T$. In summary, the SMESO design is shown in equation (6).

$$\begin{cases}e=q-z_1, s=\dot{\tilde{e}}+\Lambda\tilde{e}\\ \dot{z}_1=z_2-k_1s-\gamma_1fal(s,\alpha_1,\delta)\\ \dot{z}_2=\dot{z}_3-k_2s-\gamma_2fal(s,\alpha_1,\delta)+b_0u^*\\ \dot{z}_3=-k_3s-\gamma_3fal(s,\alpha_1,\delta).\end{cases} \tag{6}$$

In equation (6), $k>0$ and $\gamma\in R^{3\times3}$ represent diagonal positive definite matrices. Figure 3 displays the improved nonlinear ADRC.

In Figure 3, v_1 is the smoothed signal output by the tracking differentiator, v_2 is the derivative of the smoothed signal, e_1 is the error between v_1 and the observed value z_1, e_2 is the error between v_2 and the observed value z_2, u_0 is the initial control quantity output by the nonlinear feedback, and u is the final control quantity after disturbance compensation. The tracking differentiator of the improved nonlinear ADRC is calculated in equation (7).

$$\begin{cases}e_1=v_1-z_1\\ e_2=v_2-z_2\\ u_0=\beta_1nf(e_1,\alpha_0,\delta_2)+\beta_2nf(e_2,\alpha_1,\delta_2)\end{cases}. \tag{7}$$

In equation (7), δ_2 represents the filtering factor. β_1 signifies the gain coefficient of the error. β_2 signifies the gain coefficient of error differentiation. α_0 and α_1 represent nonlinear factors.

In ESO, after observing system disturbances, disturbance compensation is required to unify the internal and external disturbances as the total disturbance, and improve the control performance. The specific function is shown in equation (8).

$$u=u_0-\frac{z_3}{b_0}. \tag{8}$$

In equation (8), $\frac{z_3}{b_0}$ signifies the total disturbance compensation. u_0 signifies the control signal before disturbance compensation. u signifies the control quantity of the controlled robotic arm.

Based on the Lyapunov stability theory, stability analysis was conducted on the improved nonlinear ADRC system. The tracking errors of the system is defined as $e_1=v_1-z_1$ and $e_2=v_2-z_2$, where v_1 and v_2 are the desired states and, and z_1 and z_2 are estimated values of ESO. The Lyapunov function $V(t)=\frac{1}{2}e_1^2+\frac{1}{2}e_2^2+\frac{1}{2b_0}z_3^2$ is constructed, wherez_3 is the estimated value of ESO for the

total disturbance and β_3 is the positive definite gain coefficient. The Liapunov function is derived by substituting the system state equation (Eq. (6)) and the control law (Eq. (7)). Combined with the strict monotonicity of the nonlinear function $nf(e)$, the result $\dot{V}(t) = -e_1\beta_1 \mathrm{nf}(e_1) - e_2\beta_2 \mathrm{nf}(e_2) - \frac{1}{\beta_3} z_3(\beta_3 \mathrm{nf}(e_1) + d)$ is obtained. d is the total system perturbation. Since β_1, β_2, and $\beta_3 > 0$ and $nf(e)$ is a negative definite function, $\dot{V}(t) \leq 0$ is constant, indicating that the system is stable in the Liapunovian sense. Further analysis shows that when $t \to \infty$ and $V(t) \to 0$, i.e., the tracking error e_1, e_2 and the perturbation estimation z_3 converge to zero, the stability of the improved ADRC method is verified.

2.2 Application of industrial robotic arm based on nonlinear ADRC technology

After improving the active disturbance rejection controller mentioned above, the study applies the controller to industrial robotic arms. As the core equipment of intelligent manufacturing, industrial robotic arms are widely used in welding, assembly, handling, and other scenarios [17,18]. However, the robotic arm system has problems such as nonlinearity, strong coupling, and external interference, and traditional control methods are difficult to satisfy high-precision control requirements. Nonlinear ADRC technology provides a new approach for solving the above problems by compensating for internal and external disturbances in real time through ESO [19].

The study first constructs a dynamic model for the robotic arm, as shown in equation (9).

$$\tau = M(q)\ddot{q} + C(q,\dot{q})\dot{q} + G(q) + F_d. \tag{9}$$

In equation (9), $M(q)$ signifies the inertia matrix. $C(q,\dot{q})\dot{q}$ signifies the matrix of Coriolis force and centrifugal force. $G(q)$ signifies the gravity term. F_d represents the external disturbance. q, $\dot{q}$, and q represent the rotation angle, angular velocity, and angular acceleration vectors. τ signifies the generalized moment vector. The joint-link modeling is presented in Figure 4.

In Figure 4, the study adopts the parameter method, which is a standardized approach used to depict the relative position and attitude between connecting rods in the robotic arm. The length of the Connecting Rod (CR) is the distance from the current joint axis to the next joint axis along the previous joint axis. The torsion angle of the CR is the angle between the previous and the current joint axis. CR offset is the distance from the origin of the previous one to the origin of the current CR along the current joint axis. Joint angle is the rotation angle of the current joint axis [20,21].

According to the Lagrange equation, a dynamic equation is construed for the robotic arm system, as shown in equation (10).

$$\tau_i = \frac{d}{\mathrm{d}t}\left(\frac{\partial L}{\partial \dot{q}_i}\right) - \frac{\partial L}{\partial q_i}, i = 1, 2, \cdots, n. \tag{10}$$

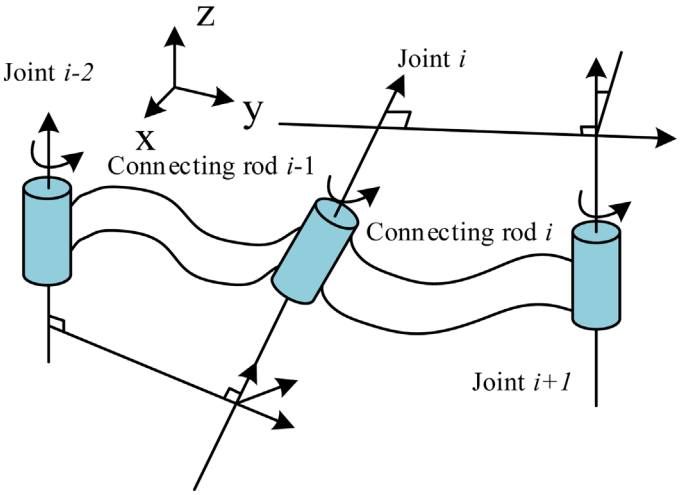

Fig. 4. Joint-link modeling of robotic arm.

In equation (10), i represents the joint. q_i signifies the generalized coordinates of the joint. $\dot{q}_i$ signifies the generalized velocity. τ_i represents the generalized moment. The transfer function between the motor output and input is shown in equation (11).

$$\frac{\Omega(s)}{U_a(s)} = \frac{K_e}{(R_a + L_a s)(f + Js) + K_e K_a}. \tag{11}$$

In equation (11), $\Omega(s)$ represents the output quantity. $U_a(s)$ represents the input quantity. K_a represents the back electromotive force constant. L_a signifies the inductance of the armature circuit. R_a signifies the resistance of the armature circuit. f signifies the coefficient of viscous friction. K_e signifies the motor torque constant. J signifies the moment of inertia. The mathematical model of motor position is shown in equation (12).

$$\frac{d^2\theta}{dt^2} = \frac{K_e K_a}{JR_a}\omega - \frac{T_d}{J} + \frac{K_e}{JR_a}u_a. \tag{12}$$

In equation (12), T_d represents the load torque with interference factors. ω signifies the angular velocity. u_a represents the armature circuit voltage. θ represents the angle at which the motor rotates.

The joints of industrial robotic arms generally use DC torque motors, as displayed in Figure 5.

In Figure 5, $\mathrm{T_d}$ (t) represents the load disturbance torque, $\mathrm{i_a}$ (t) represents the armature current, and $\mathrm{T_e}$ (t) represents the electromagnetic torque of the motor; Ra is the armature resistance, $\mathrm{L_{as}}$ is the armature inductance, $\mathrm{K_e}$ is the back electromotive force coefficient, f is the viscous friction coefficient, Js is the moment of inertia, and $\mathrm{K_a}$ is the feedback coefficient; $\mathrm{G_1(s)}$=1/(Ra+La) s) is the transfer function of the armature circuit, $\mathrm{G_2(s)}$=1/((f+J) s) is the mechanical transfer function of the motor, and Ea is the feedback signal of the back electromotive force. The overall structure principle of the DC torque motor from electrical signal input to torque, speed output, and feedback regulation is presented. It is the core component of the industrial

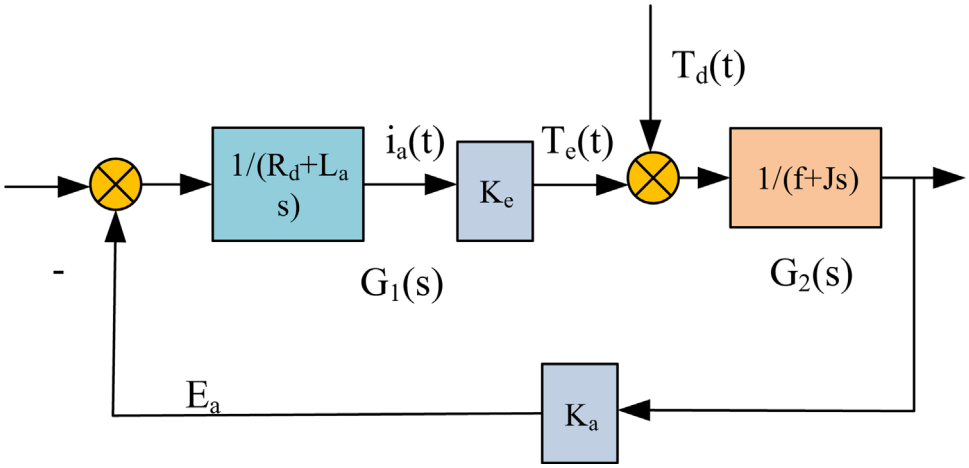

Fig. 5. Structure of DC torque motor.

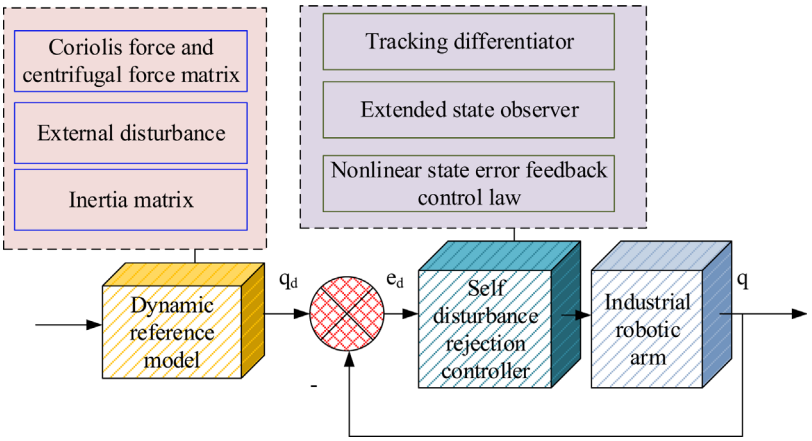

Fig. 6. Industrial robotic arm control based on dynamic model and nonlinear ADRC.

robotic arm joint drive system. By increasing the diameter of the motor rotor and shortening the magnetic circuit length, higher torque output per unit volume can be achieved. The torque can be directly controlled through current closed-loop, simplifying the control algorithm [22,23]. In practical applications, there are disturbance factors affecting the control accuracy of robotic arm joints. Therefore, the study considers all external disturbances and obtains the corresponding dynamic equation, as shown in equation (13).

$$\begin{cases} \tau = H(q)\ddot{q} + B(q,\dot{q})\dot{q} + G(q) + \tau_d \\ y = q. \end{cases} \tag{13}$$

In equation (13), τ_d represents all external disturbances. The tracking error is shown in equation (14).

$$e_d = q_d(t) - q(t). \tag{14}$$

In equation (14), q_d represents the expected angle. e_d represents the tracking error. $q(t) \to q_d(t)$ represents the optimal operating state. A filter is designed to estimate the load torque and suppress the noise impact during the motion of the robotic arm. The covariance matrix between noise and state variables is shown in equation (15).

$$\begin{cases} \begin{cases} Q = cov(w) \\ R = cov(v) \end{cases} \\ P_k = cov\{e_k e^T\} \end{cases}. \tag{15}$$

In equation (15), Q signifies the noise covariance matrix. R signifies the covariance matrix of the state variable. P signifies the covariance matrix of state estimation error. w represents the noise. v represents the adjustable noise. w_k represents the discrete state of noise. v_k represents the discrete state of adjustable noise. The control of industrial robotic arm based on dynamic model and nonlinear ADRC is presented in Figure 6.

In Figure 6, the study combines the dynamic model with ADRC and takes SMESO to estimate the total disturbance of the robotic arm in state observation, including Coriolis force, centrifugal force, external disturbances, etc. On disturbance compensation, the estimated total disturbance action is taken as a feedforward

Table 1. Related parameters.

Mechanical arm parameter project	Parameter	Project	Parameter
Model	Z1 AIR, Z1 PRO	CPU	Intel®Core(TM) i7-4790 @3.60 GHz
Freedom	6 axes	Memory	8 GB
Weight	4.3 kg, 4.5 kg	Hard drive	2 TB
Load capacity	2 kg, ≥ 3 kg	Bandwidth	100 Mb/s
Repeatability	~0.1 mm	Operating system	Linux Ubuntu 1 8.04
Interface	Ethernet	Mechanical arm User operating system	Ubuntu
Power	MAX 500 w	/	/

compensation term and added to the control input. Nonlinear feedback laws are designed based on state errors in nonlinear feedback to enhance the robustness.

3 Results

To verify the designed control method for industrial robotic arms based on nonlinear ADRC technology, experiments are conducted to validate it. The experimental data are analyzed, providing reference for the development of industrial robotic arms.

3.1 Experimental environment for verifying control methods of industrial robotic arms

The study selects an industrial robotic arm from a certain company and applies the proposed control method for industrial robotic arms based on nonlinear ADRC technology. A simulation model of an industrial robotic arm in Matlab environment is built. The experimental platform is equipped with 8 GB, 2 TB hard drives, Linux Ubuntu 18.04 system, and a 2.9 GHz Intel i5 processor. Table 1 displays the related parameters.

3.2 Analysis of the control effect of ADRC technology for industrial robotic arm

Figure 7 shows the new *nf*() function curve proposed in the study. The *nf*() function proposed in Figure 7a had good convergence properties. During system operation, the function could maintain good robustness and smoothness, which improved system stability. In Figure 7b, rounding was applied at the inflection point to address the jitter. This means that the function can provide a smoother response when dealing with dynamic changes in the system, thereby reducing system instability.

Figure 8 displays the simulation results of SMESO response curves in different signal waveforms. From Figure 8a, the step signal of the response variable showed a significant jump at 1 s. The response variables z1, z2, and z3 exhibited different dynamic response characteristics after the step signal jump. z1 and z2 quickly reached a stable value after the jump, while the response of z3 was relatively slow, showing a gradually rising and then stable trend. The sine signal in Figure 8b exhibited periodic changes within the time period of 0 to 5 s. The response variables z1, z2, and z3 of SMESO also exhibited periodic changes under the action of sinusoidal signals. The response of z1 and z2 was closer to the frequency and amplitude of a sine signal, while the response amplitude of z3 was smaller and the amplitude was slightly different. Overall, the SMESO proposed in the study was able to timely visualize nonlinear dynamics and external disturbances in the system. The state of the robot arm includes step signal parameter settings and joint motion trajectories. The step signal parameter is set to an amplitude of 0.5 rad, triggering a jump at 1 s; The joint motion trajectory adopts the typical trajectory of a 3-degree-of-freedom robotic arm (such as moving from the initial angle [0,0,0] rad to the target angle [0.8, 1.2, 0.6] rad). The simulation results show that after the step signal is triggered, the joint angle quickly tracks, verifying the response ability of SMESO to dynamic changes.

Figure 9 compares the error between Proportional-Derivative (PD) control and ADRC control before and after improvement. In Figure 9a, the error of PD control was relatively large and exhibited significant periodic fluctuations. The error of ADRC technology and the improved ADRC technology was relatively small, and the error of the improved ADRC technology was lower, showing better stability and accuracy. In Figure 9b, the error of PD control was still relatively large, and the fluctuation was more obvious, with an error of about 0.10–0.20. The error of ADRC technology and the improved ADRC technology was relatively small, within 0.18. The error of the improved ADRC technology was lower, showing better control effect. In both cases, the improved ADRC technology exhibits minimal error and optimal stability, indicating that it outperforms the other two control methods on control accuracy and stability.

Figure 10 displays the joint motion trajectory tracking error of different control methods. The research method is sliding mode control, and the traditional control method selects PD control and Neural Network (NN) for compensation. In Figure 10a, the errors of sliding mode control and NN compensation control were small, within 0.2 rad, and relatively stable. The PD control showed significant error peaks and fluctuations at approximately 10 s and 15 s, with the highest reaching 0.64 rad and the lowest reaching −0.3 rad. In Figure 10b, the errors of these three control methods were small, all less than 0.01 rad, and relatively stable. There were significant error peaks and

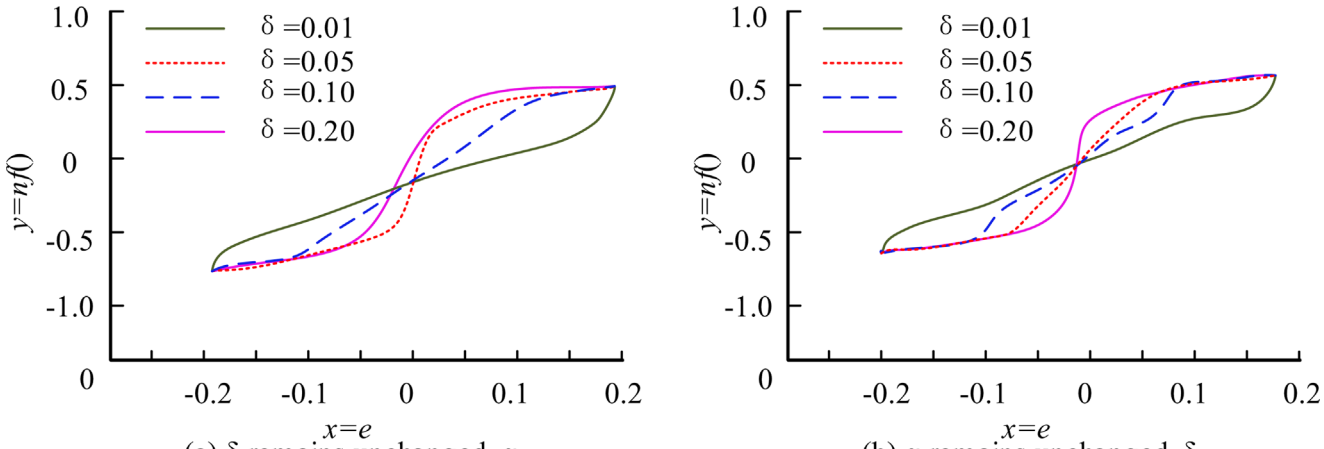

Fig. 7. Experimental verification of the proposed novel nf() function curve.

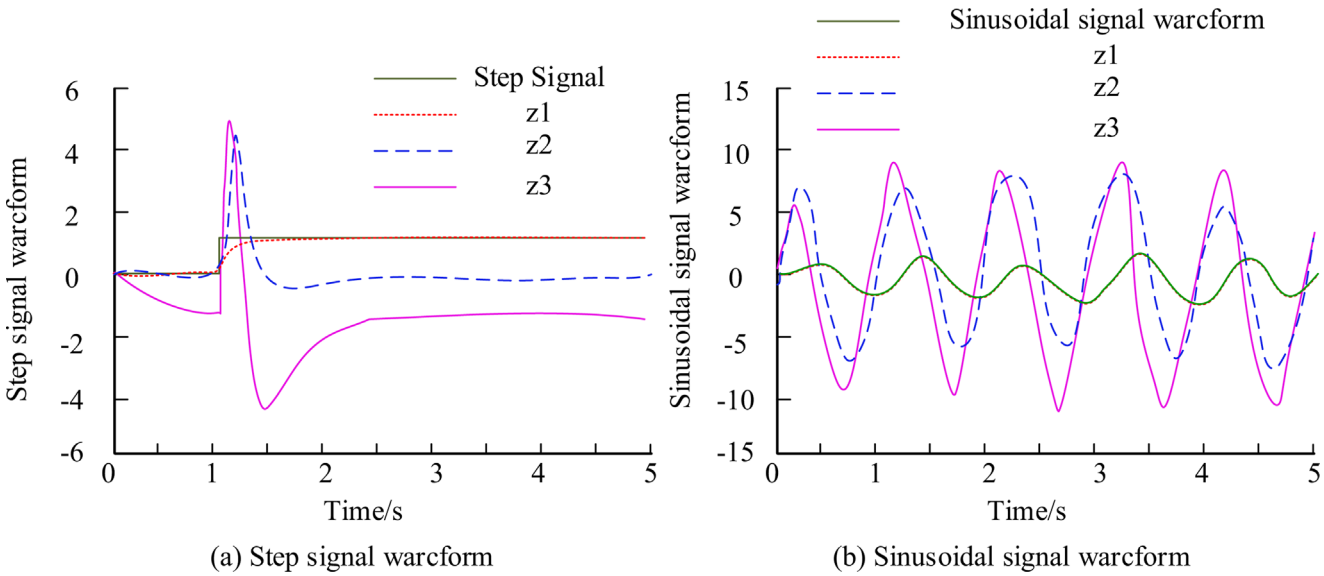

Fig. 8. Response curves of SMESO in different signal waveforms.

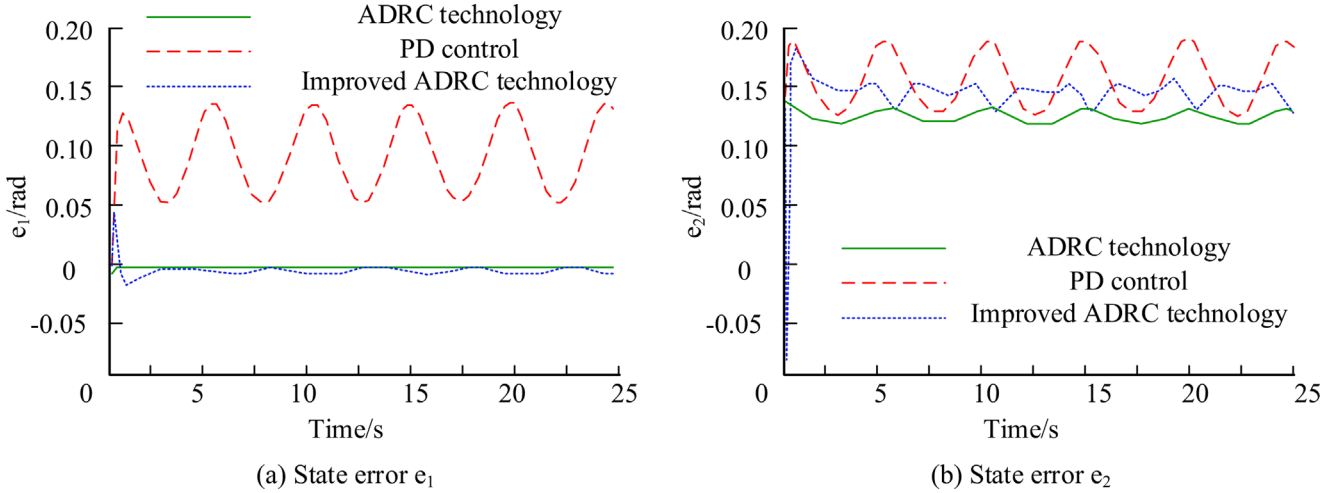

Fig. 9. Comparison of error simulation between PD control and ADRC.

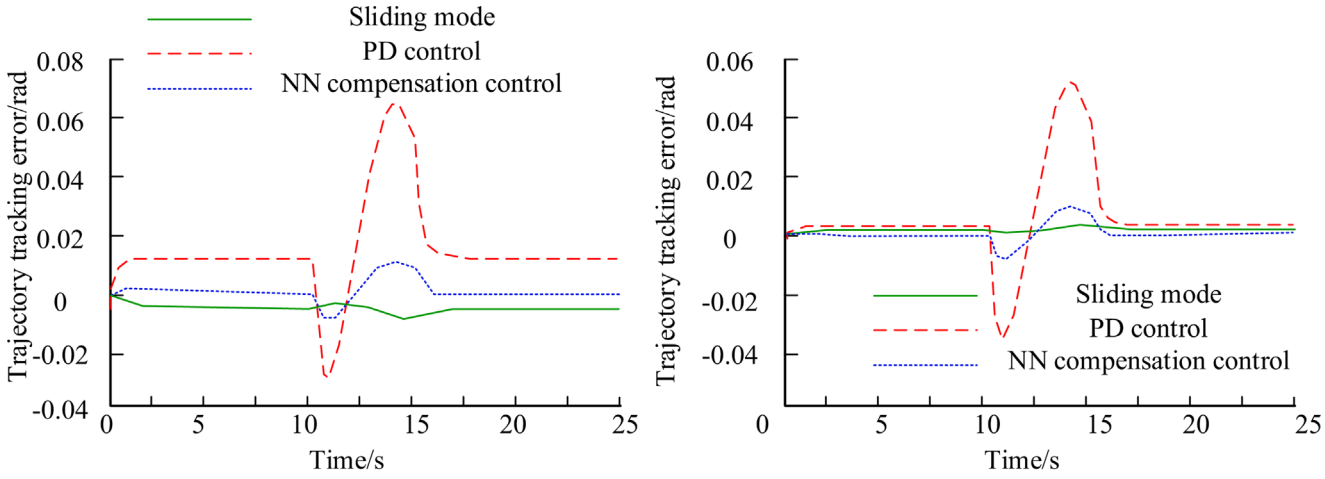

Fig. 10. Tracking errors of joint motion trajectories using different control methods.

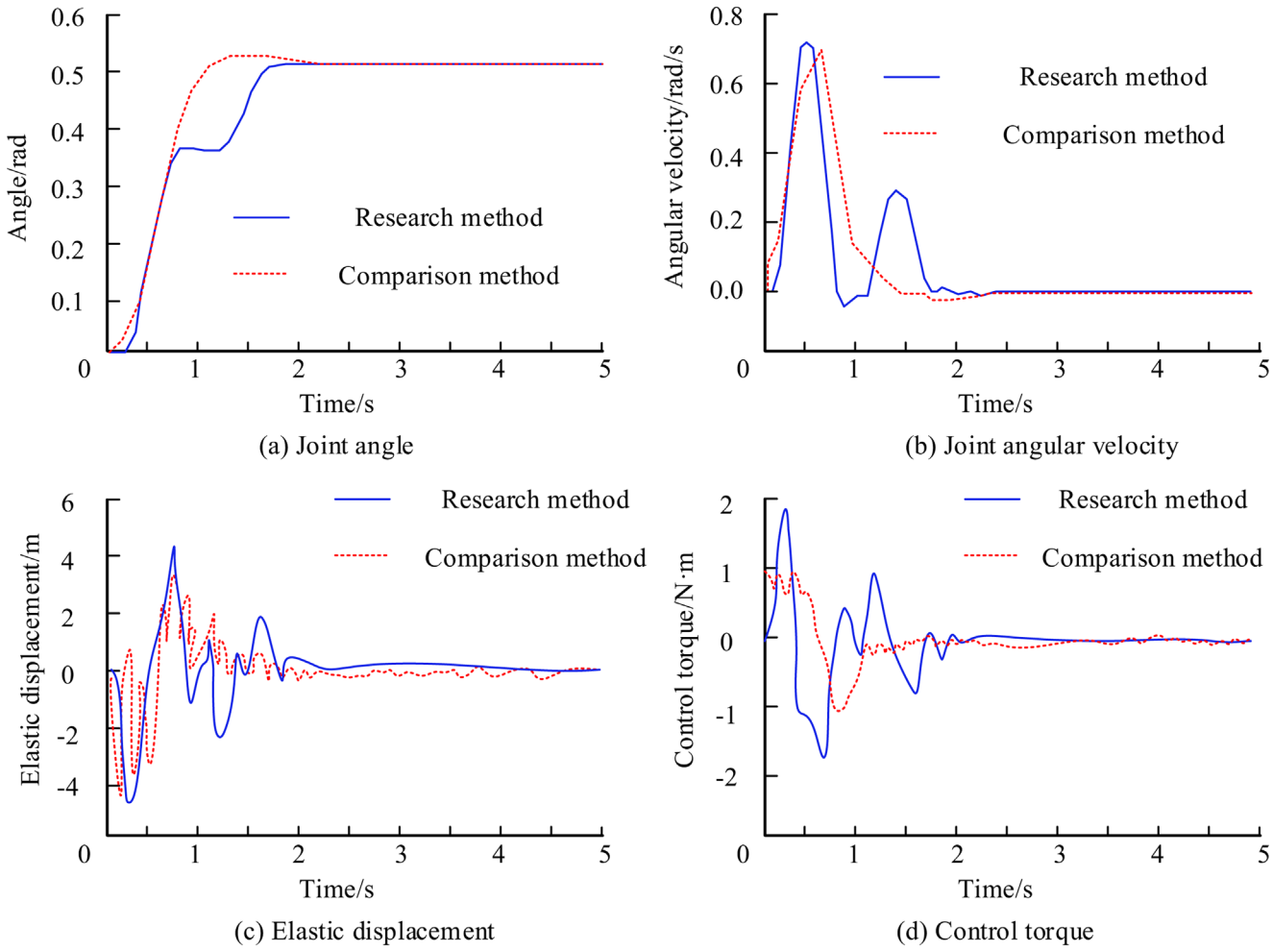

Fig. 11. Industrial robotic arm joint angle and angular velocity variation curve.

fluctuations in PD control at approximately 10 and 15 s, with the highest reaching 0.05 rad and the lowest reaching 0.035 rad. Next was PD control, while the proposed nonlinear ADRC sliding mode control had the smallest fluctuation, which was the most stable.

Figure 11 shows the experimental results of the joint angle and angular velocity variation curves of an industrial robotic arm in practical applications. In Figure 11a, the joint angle under the research method and the comparative method tended to stabilize after about 2 s. In Figure 11b,

the changes of joint angular velocity under the two methods were similar, but the joint angular velocity under the research method tended to stabilize after about 2 s, while the joint angular velocity under the comparative method tended to stabilize after about 2.5 s. In Figure 11c, the elastic displacement tended to stabilize after approximately 2.1 s, while the comparative method showed slight fluctuations after stabilizing. In Figure 11d, the control torque under the research method and the comparative method tended to stabilize after approximately 2 s. The joint angle, joint angular velocity, control torque, and change trend under the two methods were similar, but there were differences in reach a stable state and the final stable value. The research method has advantages in controlling the speed of robotic arm joints.

To verify the actual effectiveness of the algorithm, a certain model of 6-axis industrial robotic arm was selected for practical experiments. In the welding operation scenario, the tracking error data of the robotic arm end is as follows: when using traditional PD control, the average error is 0.042 rad, and the maximum error reaches 0.06 rad; When using the proposed nonlinear ADRC, the average error is reduced to 0.008 rad, the maximum error is only 0.012 rad, and there is no significant fluctuation, which is consistent with the simulation results and verifies the effectiveness of the algorithm in practical applications.

4 Discussion and conclusion

Nonlinear system control has always been an important research direction in robotics, automation systems, and many other engineering fields. Especially in robotic arms, it is particularly difficult to achieve stable and accurate control systems due to the highly nonlinear and unknown constraints of the system. Therefore, a control method for industrial robotic arms based on nonlinear ADRC technology was designed. Based on ESO to estimate and compensate for total interference, high-precision trajectory tracking was achieved using NLSEF control law. The errors of sliding mode control and NN compensation control were small, within 0.2 rad, and relatively stable. The PD control showed significant error peaks and fluctuations at approximately 10 s and 15 s, with the highest reaching 0.64 rad and the lowest reaching −0.3 rad. The errors of the three control methods were relatively small, all less than 0.01 rad, and they were relatively stable. PD control showed significant error peaks and fluctuations at approximately 10 s and 15 s, with the highest reaching 0.05 rad and the lowest reaching 0.035 rad, followed by PD control. The nonlinear ADRC sliding mode control had the smallest fluctuations and was the most stable. The method can effectively address the control challenges of industrial robotic arms under complex working conditions, significantly improve the dynamic performance and robustness, and has broad application prospects. However, the research on multi-modal switching of robotic arms in complex tasks such as precision assembly and compliant operation is still insufficient. In the future, the ADRC parameter tuning method is further optimized to improve the adaptive capability of control systems.

Funding

This research did not receive any specific grant from funding agencies in the public, commercial, or not-for-profit sectors.

Conflicts of interest

The authors report there are no competing interests to declare.

Data availability statement

Data will be available on a reasonable request.

Author contribution statement

Zhiwei Geng and Teng Wan wrote the main manuscript text, Zhiwei Geng collected the data and prepared tables. Teng Wan did the data analysis. Zhiwei Geng designed and conducted the research. All authors reviewed the manuscript.

References

1. P.H. Kuo, M.J. Syu, S.Y. Yin, H.H. Liu, C.Y. Zeng, W.C. Lin, Intelligent optimization algorithms for control error compensation and task scheduling for a robotic arm, Int. J. Intell. Robot. Appl. **8**, 334–356 (2024)
2. Y. Zhao, M. Zhang, H. Wu, S. Jing, T. Zhou, M. Todoh, A comprehensive sensorimotor control model emulating neural activities for planar human arm reaching movements, Appl. Intell.: Int. J. Artifi. Intell. Neural Netw. Compl. Probl. −Solv. Technol. **54**, 2508–2527 (2024)
3. W. Zhao, Y. Sun, H_∞ control of switched Lurie systems with dwell time, Proc. Inst. Mech. Eng. Part I. J. Syst. Control Eng. **238**, 1112–1122 (2024)
4. C. Yuan, L. Guo, X. Zhang, X. Lai, W. Lu, Novel active disturbance rejection-based sliding-mode control for permanent magnet linear synchronous motor drives, IEEJ Trans. Electr. Electron. Eng. **19**, 119–129 (2023)
5. M.S. Ben, M. Belkhiri, A. Belkhiri et al., Active disturbance rejection control of flexible industrial manipulator: A MIMO benchmark problem, Eur. J. Control, **77**, 1–10 (2024)
6. E. Nuo, I. Sarras, H. Yin, B. Jayawardhana, Consensus of Euler-Lagrange agents with internal model disturbance rejection and interconnection delays, IEEE Trans. Autom. Control **69**, 4066–4071 (2024)
7. M. Flores-Padilla, C. Treesatayapun, Adaptive controller based on the affine equivalent model with disturbance rejection for discrete-time switched systems, Int. J. Syst. Sci.: Theory Practice Math. Modell. Simul. Optimiz. Control Relation Biol. Econ. Indust. Transport. Syst. **54**, 3059–3070 (2023)
8. H. Xie, L. Li, X. Song, W. Xue, K. Song, Parameter self-learning feedforward compensation-based active disturbance rejection for path-following control of self-driving forklift trucks, Asian J. Control **25**, 4435–4451 (2023)
9. S. Yao, W. Yi, M. Haifeng, L. Xichang, Compensation control of hydraulic manipulator under pressure shock disturbance, Nonlinear Dyn. **11**, 11153–11169 (2023)

10. S. Luo, G. He, N. Hou, Reflux power optimization of a dual-active hybrid full-bridge converter based on active disturbance rejection control, Energies **17**, 4299–4300 (2024)
11. A. Jing, J. Wang, J. Gao, Y. Chen, Y. Cao, Y. Cao, Self-tuning adaptive active disturbance rejection pitch control of a manta-ray-like underwater glider, Ocean Eng. **254**, 1–111364.11 (2022)
12. A. Wellendorf, P. Tichelmann, J. Uhl, Performance analysis of a dynamic test bench based on a linear direct drive, Arch. Adv. Eng. Sci. **1**, 55–62 (2023)
13. Z. Cheng, L. Songxiao, Z. Zhuo, Industrial robot arm dynamic modeling simulation and variable-gain iterative learning control strategy design, J. Mech. Sci. Technol. **38**, 3729–3739 (2024)
14. I. Choi, S.J. Yoon, Y.L. Park, Linear electrostatic actuators with Moire-effect optical proprioceptive sensing and electroadhesive braking, Int. J. Robot. Res. **43**, 646–664 (2024)
15. M. Armstrong-Hough, P. Lin, S. Venkatesh, M. Ghous, C.L. Hough, S.H. Cook, Ethnic disparities in deep sedation of patients with acute respiratory distress syndrome in the united states: secondary analysis of a multicenter randomized trial, Annals Am. Thoracic Soc. **21**, 620–626 (2024)
16. M.S. Ryan, Does the use of antimicrobials in different periodontal treatment strategies result in better treatment outcomes? − A radiographic analysis, Evid. −Based Dent. **25**, 31–32 (2024)
17. F. Ito, Y. Ishii, S. Kurumaya, K. Kagaya, T. Nakamura, A design method for instantaneous force generation based on a mantis shrimp with exoskeleton spring, IEEE/ASME Trans. Mechatron.: Joint Publ. IEEE Indust. Electron. Soc. ASME Dyn. Syst. Control Division **29**, 960–971 (2024)
18. X. Geng, Y. Zheng, Y. Li, Z. Li, Early radiographic and clinical outcomes of robotic-arm-assisted versus conventional total knee arthroplasty: a multicenter randomized controlled trial, Orthopaedic Surgery **16**, 2732–2740 (2024)
19. Y. Sun, X. Dai, Q. Yin, L. Ju, X. Tang, M. Li, Design and control of ultrasound image-guided prostatic brachytherapy robot, Recent Patents Mech. Eng. **17**, 116–122 (2024)
20. T.H. Nguyen, D.T. Nguyen, V.H. Tran, T.T. Mac, A study on rocker arm defect inspection based on vision system, Int. J. Modern Phys. B. Condens. Matter Phys. Stat. Phys. Appl. Phys. **38**, 1–2440024.12 (2024)
21. J. Hye, L. Jewoo, C. Kyu-jin, Arm back support suit (AbsSuit) for parcel delivery with a passive load redistribution mechanism, IEEE Robot. Autom. Lett. **9**, 1238–1245 (2024)
22. T. Cartier, G. Rao, E. Viehweger, L. Vigouroux, Evolution of muscle coordination and mechanical output throughout four weeks of arm cranking submaximal training, J. Neurophysiol. **129**, 541–551 (2023)
23. S.Y. Yang, K.Y. Kim, J.U. Ko, S.W. Seo, S.T. Hwang, J.H. Park, H.S. Jung, Y.J. Gong, J.W. Suk, H. Rodrigue, H.P. Moon, J.C. Koo, J.D. Nam, H.R. Choi, Design and control of lightweight bionic arm driven by soft twisted and coiled artificial muscles, Soft Robot. **10**, 17–29 (2023)

Cite this article as: Zhiwei Geng, Teng Wan, Nonlinear active disturbance rejection control for industrial robotic arm and its application, Int. J. Metrol. Qual. Eng. **16**, 9 (2025), https://doi.org/10.1051/ijmqe/2025009